Chapter 4

Ammonia gas sensitivity and broadband photo-detection by depleted layer of polymer/QDs based thin film transistor

Abstract

An ambient temperature broadband photo-detector and ammonia (NH_3) gas sensor devices are developed with PBTTT-C14/WS_2-QDs heterojunction thin film. Gas and photo-sensitive semiconducting composite thin layer of PBTTT-C14 conjugate polymer and hydrothermally synthesized WS_2-QDs have been deposited by high yield and cost-effective 'floating film transfer method' (FTM), which works as a channel (p-type) of the thin film transistor (TFT). To determine the NH_3 sensing behavior of the TFT, different concentrations have been exposed of NH_3 (0.5-20 ppm) on the channel of the TFT, which shows the response of ~50% at 10 ppm ammonia concentration, which is significantly higher than PBTTT-C14 only TFT. This improvement is made possible by the NH_3-responsive depleted layer of polymer/QDs heterojunction, which varies widely in the presence of ammonia. As a consequence, the ON/OFF ratio, carrier mobility and threshold voltage (V_{th}) of the device changes in a wider range. Besides, this TFT based gas sensor is also highly selective to the other interfering gases. In addition to NH_3 gas sensitivity, this TFT also shows very high photosensitivity under white light illumination that enhances 'ON' and 'OFF' current of the device by ~2.2 and 70 times, respectively under one sun white light illumination, whereas V_{th} of the device is shifted by ~22 V. Besides, the device shows quite fast response/ recovery time under NH_3 gas exposure and light illumination.

4.1. Introduction

Environmental pollution caused by the production of nitrogenous fertilizers and other chemicals are the main source of typical atmospheric pollutant ammonia (NH_3), which is generated mostly by ammonification and combustion [136, 137]. Explosion of poisonous NH_3 gas can cause severe damage to an individual's health even at lower concentrations (ppb or ppm level). The corrosive

nature of NH_3 can cause damage to the lungs, eyes, skin and can induce pulmonary edema, blindness etc. Inhaling excessive amounts of this colorless with pungent odor gas can be a source of serious diseases like dyspnea and cancer [136, 138, 139]. This hazardous NH_3 is primarily produced in the production unit of nitrogenous fertilizers, industrial refrigerants, and manure from the natural breakdown of dead animals and plants [5, 6]. Therefore, it is important to design an ambient temperature operating, highly responsive, and economical NH_3 gas sensor. Besides, photo-detectors are widely used for various applications like optical fiber communication, wireless communication, image sensors etc [140, 141]. Thus, a low cost, highly sensitive, and reliable photo-detector is highly demanding [142, 143].

Till date, numerous types of materials have been used for the detection of NH_3 [144, 145]. Conventional metal oxide semiconductor (MOS) based sensors performed excellently as sensitive materials with good response, but their requirement of high temperature for the detection confines their application as sensing materials [146, 147]. Various types of conducting polymers have also been used for NH_3 detection at ambient temperature. However, pure conducting polymer based sensors possess low sensing response towards NH_3. Additionally, their low conductivity, poor stability and slow response times are the key issues. Therefore, researchers have investigated the strategy of making organic/inorganic hybrid nano-composite based materials by combining metal oxides or noble metals with conducting polymers to make them more efficient sensor devices [83, 148, 149]. Recently, quantum dot (QD) of different 2D materials like; reduced graphene oxide (RGO), MoS_2, WS_2 based materials achieved more attention in recent times as a photo-detector and chemical sensor application due to their high in extinction coefficient and chemically active sites [114, 150]. Although the sensitivity of those 2D-QD only devices are limited [151]. Relatively hybrid materials of 2D-QD with other classes

of semiconductors like; organic, metal oxide or silicon are getting more attention due to their enhanced photo and gas sensitivity [152-155].

To explore the beneficial sides of organic polymers and quantum dots, I have prepared PBTTT-C14/WS_2-QDs nano-heterojunction based TFT and systematically investigated its ammonia gas and photo sensing capabilities. PBTTT-C14 is a polythiophene based π-conjugated polymer which can be a good choice for higher air stability with high carrier mobility due to its relatively deep HOMO level [123]. Besides, WS_2 is a widely studied sensor material for its exciting photoelectric and gas sensing capabilities. Keeping in view of the above facts, in this work, our main approach is to determine the NH_3 gas sensitivity of PBTTT-C14/WS_2-QDs nano-heterojunction based thin film transistor (TFT) sensor at room temperature. Besides, a broadband photosensitivity of this TFT has been investigated. This composite based TFT was successfully fabricated *via* a cost-effective and facile procedure floating film transfer (FTM) method and the capability of ammonia and broadband photo sensing of this device are systematically investigated. The TFT channels of the prepared sensors are exposed with different ammonia concentrations (0.5 - 20 ppm), which shows fast response and recovery times with exceptional sensitivity and repeatability. In our previous study, it was observed that the PBTTT-C14/MoS_2-QDs composite based TFT sensor had quite higher sensitivity with respect to the pristine PBTTT-C14 based TFT sensor, which reveals the benefit of using organic/inorganic nano-heterojunction[156]. The key improvement of this PBTTT-C14/WS_2-QDs nano-heterojunction based TFT w.r.t the earlier work is the level of sensitivity which is several-fold higher than earlier. Besides, it was observed that the PBTTT-C14/MoS_2-QDs based sensor had a relatively poor recovery time towards NH_3 gas. However, sensor based on PBTTT-C14/WS_2-QDs exhibited prompt responsiveness to the NH_3 gas and demonstrated rapid response and recovery

following each gas pulse. The duration of the recovery is estimated to be between 5 and 6 s with exhibiting acceptable repeatability in terms of analyte concentrations. Further, the origin of the sensing mechanisms for the improvement of the device sensitivity has been discussed. In addition to its application as NH_3 gas sensor, this manuscript has also demonstrated its application as a visible range broadband photo-detector with a satisfactory sensitivity.

4.2. Materials and experimental methods

4.2.1. Synthesis of WS_2-QDs

Highly pure sodium tungstate dihydrate ($Na_2WO_4 \cdot 2H_2O$), L-cysteine, and hydrochloric acid precursor materials acquired from Merck, India have been used for the hydrothermal synthesis of WS_2-QDs.The procedure is similar as shown in previous chapter 3. At the beginning of this process, sodium tungstate dihydrate and L-cysteine (2:1 w/w) were stirred separately for 20 min in 25 ml of DI water. After that, both solutions were mixed and stirred with an added amount of concentrated HCl at a maintained value of pH ~3. And finally, the as-prepared solution was transferred into a 100 ml capacity Teflon autoclave walled with stainless steel and kept for approx 42 hours at ~ 200°C in the oven. After cooling down to room temperature, the WS_2-QDs contained light yellowish solution was obtained.

4.2.2. Synthesis of PBTTT-C14/WS_2-QDs nano-composite

The poly (2,5-bis (3-tetradecylthiophen-2yl) thieno (3,2-b) thiophene) PBTTT-C14 (Sigma-Aldrich Pvt. Ltd, Mol. Wt. > 40,000) has been used for PBTTT-C14/WS_2-QDs nano-heterojunction thin film fabrication that works as semiconducting channel materials of TFT. On the other hand, hydrothermally synthesized WS_2-QD has been dispersed in a chloroform ($CHCl_3$) solution. To transfer WS_2-QDs from the aqueous solution to the $CHCl_3$, we have used the phase

transfer technique, as reported in our earlier work [156]. In this method, aqueous solutions of QDs were sonicated rigorously for 2-3 hours with the same quantity of $CHCl_3$. In this immiscible solution of chloroform and water, the aqueous dispersion will remain at the top, and heavy $CHCl_3$ will remain at the bottom. After the completion of the sonication procedure, from the top, the aqueous solution was discarded, and the remaining solution will contain the QDs in chloroform.

After transferring QDs in $CHCl_3$ solvent, for the PBTTT-C14/WS_2-QDs nano-composite synthesis, 10 µl of $CHCl_3$/QDs dispersion was mixed in 2 mg polymer/chloroform solution with 10 mg ml^{-1} concentration. For the uniform mixing of QDs in polymer, the composite solution is sonicated and used for organic/inorganic hybrid semiconductor thin film deposition via FTM method, as described in our previous publication [24]. During this thin film deposition, a small drop of PBTTT-C14/WS_2-QDs solution was dropped under ambient conditions onto an aqueous mixture (ethylene glycol and glycerol in 3:1) containing petri-dish. Subsequently, nano-composite solution spread over the liquid medium without mixing into it and stabilized as a floating film on the liquid. Then, as prepared film on the surface of the liquid has been transferred onto the cleaned Si/SiO_2 substrate and heated at ~85°C. During this procedure, the quantity of nano-composite solution was optimized to obtain a good quality film that can be utilized to fabricate high performance TFT devices. This nano-composite film over the aqueous medium has been transferred onto the carbon coated TEM grid and Si/SiO_2 substrate for the TEM and AFM characterization purposes, respectively.

4.2.3. Device fabrication

For the TFT fabrication, highly doped silicon (p^+-Si) substrates with a SiO_2 (thermally grown) layer of 300 nm (C_{ox}, capacitance per unit area, 10 $nFcm^{-2}$) are used as the gate dielectric. Before PBTTT-C14/WS_2-QDs thin film deposition, Si/SiO_2 substrates were properly cleaned with soap solution. Afterward, substrates were cleaned in a sequence with DI water, acetone, and isopropanol by using an ultrasonic bath followed by the drying process. After the completion of the cleaning process, the composite (semiconducting) layer was deposited via pre-explained FTM method onto the cleaned Si/SiO_2 substrate followed by the drying process at ~80°C before the electrode deposition. Finally, around 60 nm source–drain Gold (Au) electrodes were subsequently deposited by thermal deposition onto the nano-composite film coated substrate with the rate of evaporation 1 Å/s to 2 Å/s at vacuum level 6×10^{-5} Torr. The interdigitated shadow masks (length (L) and width (W) of 50 µm and 18 mm, respectively) were used for the electrode deposition.

4.2.4. Characterization tools

For the characterization purpose, the absorption spectra of WS_2-QDs were obtained by UV–Vis spectrophotometer (UV-2600, Shimadzu). Electron micrographs and selected area electron Diffraction (SAED) pattern of polymer/QDs film were obtained via transmission electron microscope (TEM) study [TECHNAI $G^2$20 TWIN (New Zealand)]. The roughness study of the film was done by Atomic force micrograph (AFM) using NT-MDT "NTEGRA Prima" (Russia). Lastly, the ammonia sensing behaviors of the fabricated TFT were carried out by a controlled atmosphere gas sensing assembly. The gas assembly has two inlets and one outflow. The first inlet is for ammonia gas injection, while the second inlet and exit are for air flushing into and out of the chamber. A probe station connects a semiconductor parameter analyzer (Keysight,

B1500A) to the gas chamber. Ammonia gas with concentrations ranging from 0.5 ppm to 20 ppm is fed into the gas chamber at 27°C with 50% RH under the controlled flow of dry air, and the resulting changes in drain current are detected using electrical measurements. Similar procedure was obtained for the other sample gases preparation for selectivity analysis [125]. Photosensitivity of the device has been investigated by doing electrical characterization of the TFTs under white light illumination. Xenon lamp has been used as a source of white light.

4.3. Results and discussion

4.3.1. Characterization of WS_2 -QDs

The characteristics of synthesized WS_2-QDs were examined by TEM and UV-Vis spectroscopy. TEM image of the well dispersed QDs in water is shown in Fig. 4.1(a) and indicates that QDs are homogeneously distributed on a carbon coated Cu grid. Fig. 4.1(b) shows HR-TEM the SAED pattern (inset), which suggests that QDs are polycrystalline in nature. The size distributions of the QDs are in the range of 4-6 nm, which is observed from the histogram presented in Fig. 4.1(c). Fig. 4.1(d) demonstrates the UV-Vis spectra of WS_2-QDs with two absorption peaks at 305 nm and 383 nm. This absorption data demonstrates the excitonic characteristic of the synthesized WS_2-QDs [157, 158]. The band gap of the synthesized QDs calculated by the tauc's plot is 3.79eV represented in the inset of Fig 4.1(d).

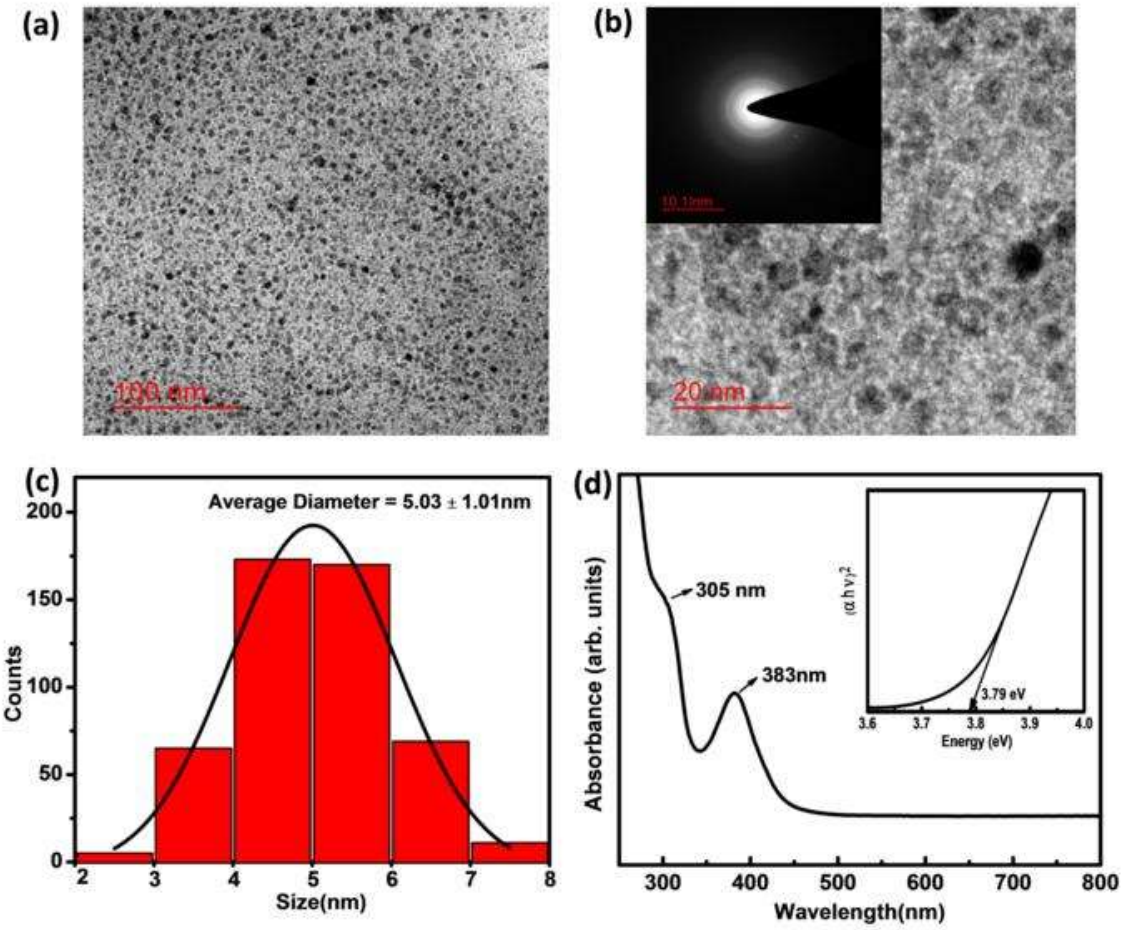

Fig. 4.1. (a) TEM image, (b) HR-TEM image and SAED pattern (inset), (c) size distribution histogram, and (d) UV-Vis spectra and Tauc's plot (inset) of synthesized WS_2-QDs.

4.3.2. Characterizations of PBTTT-C14/WS_2-QDs nano-composite thin Film

For the TEM micrograph and SAED pattern of PBTTT-C14/WS_2-QDs nano-composite, thin film has been transferred via pre-described FTM method onto the Cu grid. The TEM image of the nano-composite indicates that the QDs are distributed equivalently on the matrix of polymer, as shown in image Fig. 4.2(a). The hazy ring pattern in the SAED pattern of the nano-composite presented in Fig. 4.2(b) is due to the polymer matrix present in the nano-composite material.

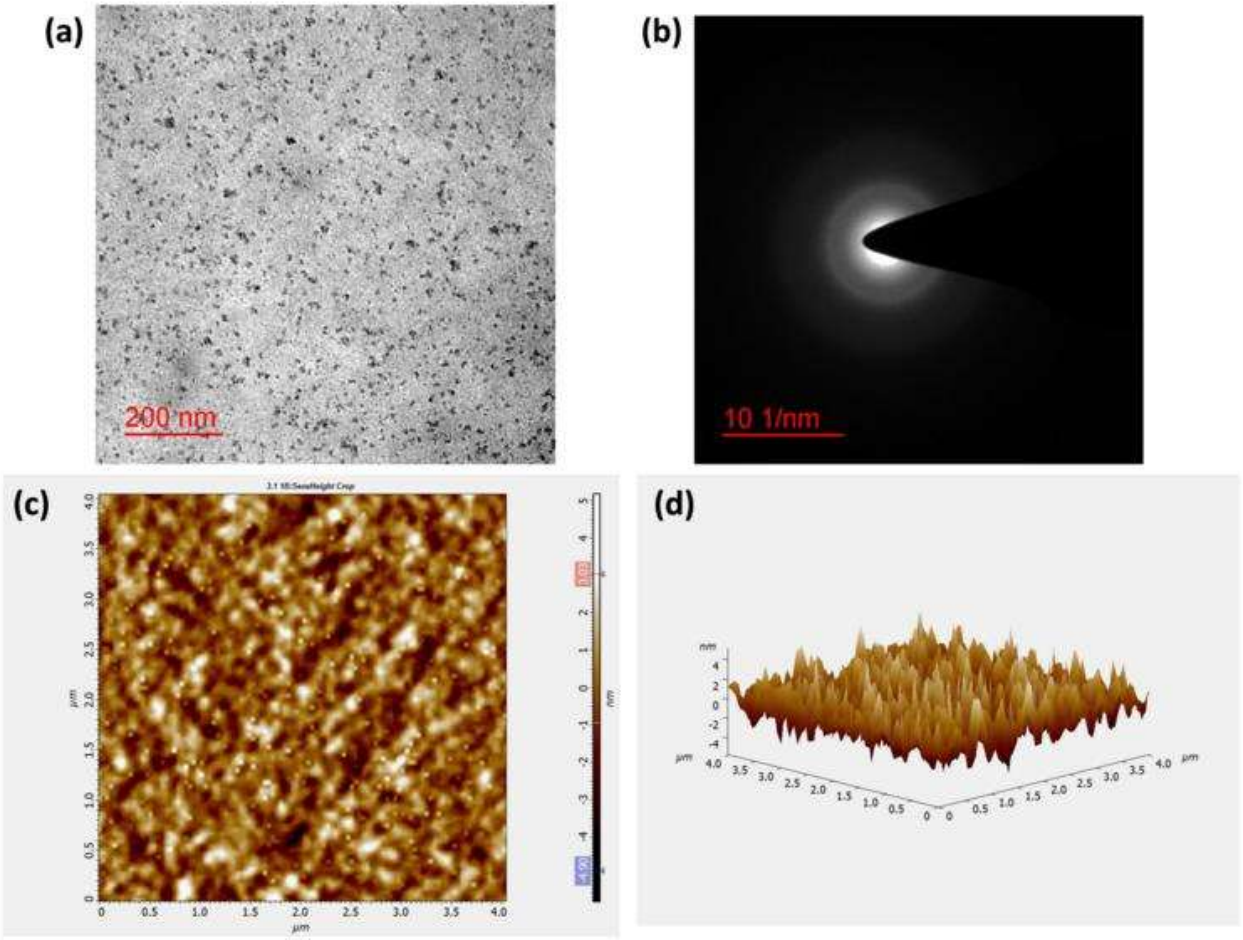

Fig. 4.2. (a) TEM micrograph and (b) SAED pattern ;(c) 2D and (d) 3D AFM image of PBTTT-C14/WS_2-QDs FTM film.

An AFM measurement has been used to analyze the surface roughness of the nano-composite film. Fig. 4.2(c) and 4.2(d) represent 2D and 3D AFM images of the polymer/QDs nano-composite film, indicating the root-mean-square (R_{rms}) roughness nano-composite film is 1.28 nm. Brighter spherical spots of this film are the WS_2-QDs, which are ~9 % surface coverage of the film, has been estimated from Image-J software (Fig. 4.2(a)). It can be noted that the WS_2-QDs have been distributed throughout the film uniformly.

4.3.3. Electrical Characterizations

For the electrical characterization of the fabricated TFT (Fig. 4.3(a)), the output (I_{DS}-V_{DS}) and transfer (I_{DS}-V_{GS}) characteristics were measured at 27°C (room temperature) with 50% relative humidity (RH) and represented in Fig. 4.3(b) and Fig. 4.3(c), respectively. Output characteristic of the TFT was examined by sweeping the drain voltage (0 to -30 V) with different constant bias gate voltages. Whereas, the transfer characteristic was estimated at a constant drain voltage of -30 V and a gate voltage sweep from 0 to -30 V.

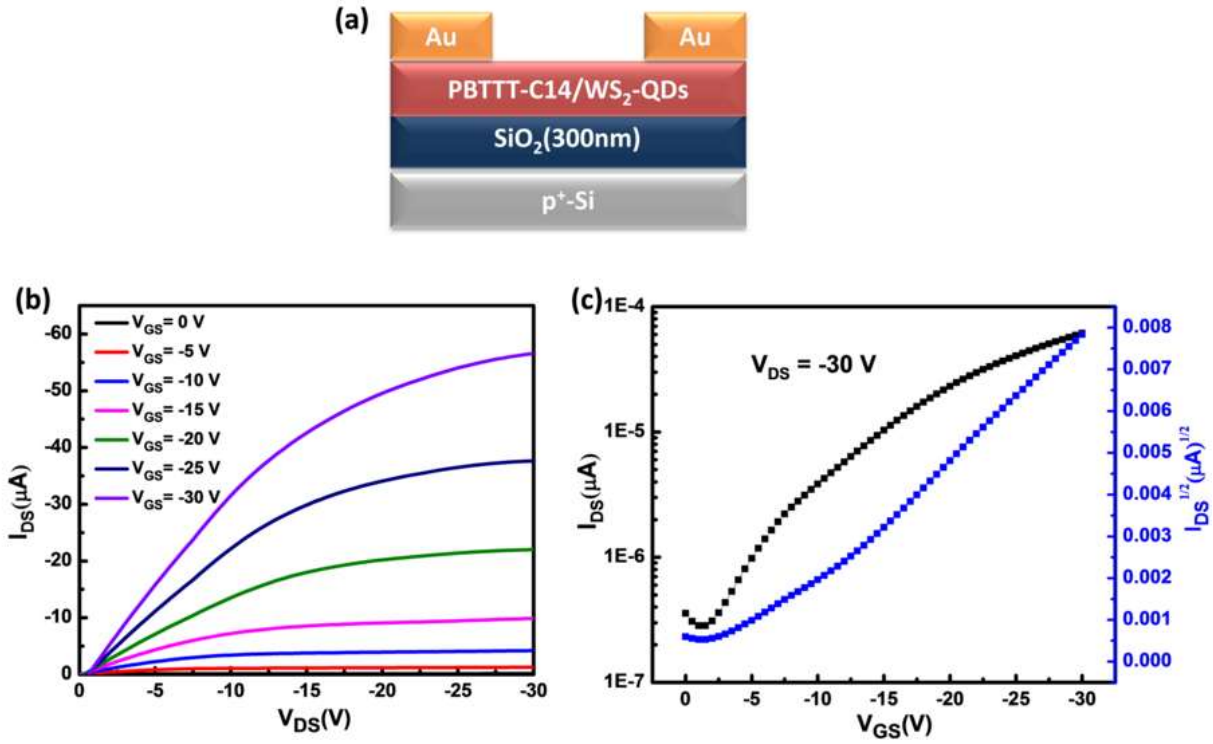

Fig. 4.3. (a) Schematic diagram, (b) Output characteristics, and (c) Transfer characteristics of PBTTT-C14/WS_2-QDs based TFT.

From the transfer characteristic, the parameters of the TFT can be extracted by using the subsequent equation (3.1).

4.3.4. Ammonia Sensing

For the gas sensing measurement, a fabricated TFT device is exposed with different concentrations of NH_3 gas ranging from 0 ppm to 20 ppm at 27°C under the controlled flow of dry air inside a sealed chamber with 50% RH. During the sensing measurement, the gate bias (V_{GS}) is swept from 0 to -30 V under a constant drain voltage (V_{DS}) of -30 V, as shown in Fig. 4.4(a). It is observed from the transfer characteristic that as soon as the concentration of NH_3 increases, the drain current (I_{DS}) of the TFT decreases gradually. The reduction in the I_{DS} (ΔI_{DS}) at constant V_{GS} can be determined by taking the difference between the I_{DS} data before and after exposure of the ammonia.

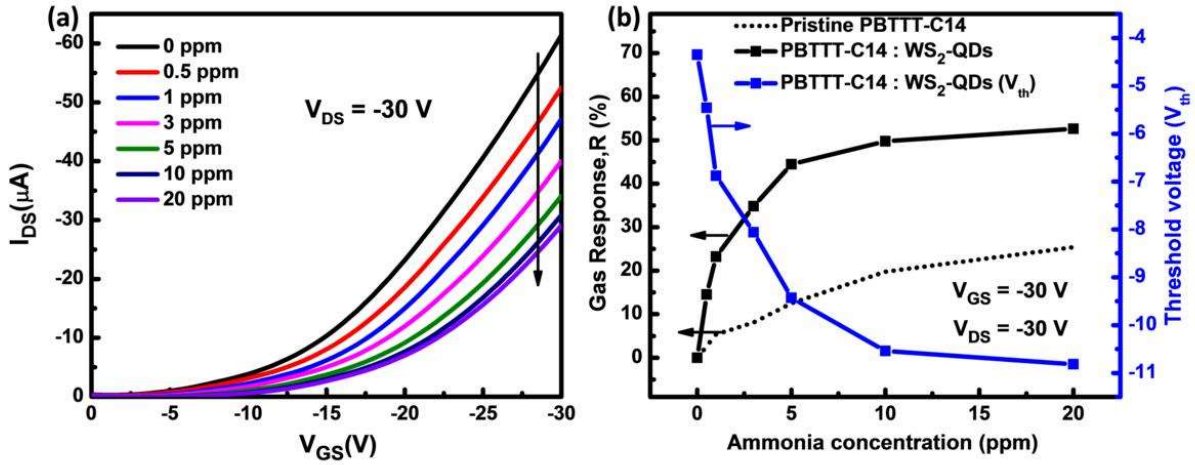

Fig. 4.4. (a) Transfer characteristics of PBTTT-C14/WS_2-QDs nano-composite film based TFT based sensor at V_{DS} = -30V and (b) Gas response (V_{GS} = -30 V, and V_{DS} = -30 V) and threshold voltage (V_{th}) shift with different concentrations of ammonia (0 ppm-20 ppm). (Response data for pristine PBTTT-C14 based TFT sensor has been added as reference (dotted line)).

Table - 4.1: The Summary of variation in TFT parameters and the sensitivity of PBTTT-C14/WS_2-QDs with different concentrations of NH_3.

NH_3 (ppm)	On current I_{on} (μA)	Effective Mobility μ_h ($cm^2V^{-1}sec^{-1}$)	Threshold voltage V_{th} (V)	Change in Threshold voltage (ΔV_{th})	Response (%)
0	-61.39	0.0536	-4.35	0	0
0.5	-52.47	0.0496	-5.46	1.11	14.53
1	-47.13	0.0481	-6.88	2.53	23.23
3	-40.02	0.0456	-8.06	3.71	34.81
5	-34.09	0.0431	-9.43	5.08	44.46
10	-30.86	0.0428	-10.54	6.19	49.73
20	-29.08	0.0425	-10.82	6.47	52.62

Besides, various electrical parameters of the device also change upon exposure of NH_3 gas, such as mobility (μ_h) and threshold voltage (V_{th}), as represented in Table - 4.1. These large variations in the electrical parameters of the fabricated TFT indicate its potential for NH_3 gas sensing application. Fig. 4.4(b) depicted the dynamic ammonia gas response (V_{GS} = -30 V, and V_{DS} = -30 V) and the corresponding shift in the V_{th} of the fabricated TFT against different NH_3 concentrations ranging from 0 to 20 ppm. Besides, response data of reference pristine PBTTT-C14 based TFT has been presented in a dotted black line. From Fig 4.4(b), it can be observed that the improvement of response w.r.t the pristine TFT is several folds higher throughout the range. This data also shows a shift of $V_{th,}$ for the nano-composite material, which is more than 6 V during the variation of NH_3 concentration that has good linearity up to 10 ppm. Besides, the

effective carrier mobility of the fabricated sensor is also reduced from 0.054 to 0.043 $cm^2 V^{-1}sec^{-1}$, which is ~20% of its original value.

4.3.5. Response, Detection limit, and Transient response

Fig. 4.5(a) depicted the dynamic ammonia gas response of the fabricated TFT based gas sensor against the different concentrations ranging from 0 to 20 ppm. The gas response (V_{DS} = -30 V and V_{GS} = -30 V) over some ammonia concentration of the fabricated TFT sensor can be extracted by the equation (3.2). From the response graph, it is clearly visible that the nano-composite based sensing layer illustrates the remarkable sensitivity in lower as well as higher concentration ranges of ammonia. However, this gas sensor has a relatively higher response of 52.62% in lower concentration range up to 20 ppm of ammonia.

The detection limit, which is one key figure of merit of the sensor, is defined by the lowest concentration of the analyte gas that can be detected, and estimated from the equation (3.3). The calculated LOD value of this sensor is ~0.44 ppm, indicating its applicability in lower concentration range of NH_3.

Fig. 4.5(b) represents cycles of the real-time transient response of the fabricated gas sensor (V_{DS} = -30 V and V_{GS} = -30 V) against the different concentrations of ammonia at 27°C. The response of the fabricated TFT sensor increases in a stepwise trend with the increasing concentration of ammonia. From this transient response curve, the response/recovery characteristics of the fabricated sensor can be determined. This data indicates that the fabricated nano-composite based TFT sensor exhibits a response time of ~2 sec, which is sufficiently fast as an NH_3 gas sensor, and the fabricated device shows a recovery time of ~6 sec for full recovery. However, it was observed that in our earlier report, the PBTTT-C14/MoS_2-QDs based sensor had a relatively poor recovery time towards NH_3 gas.

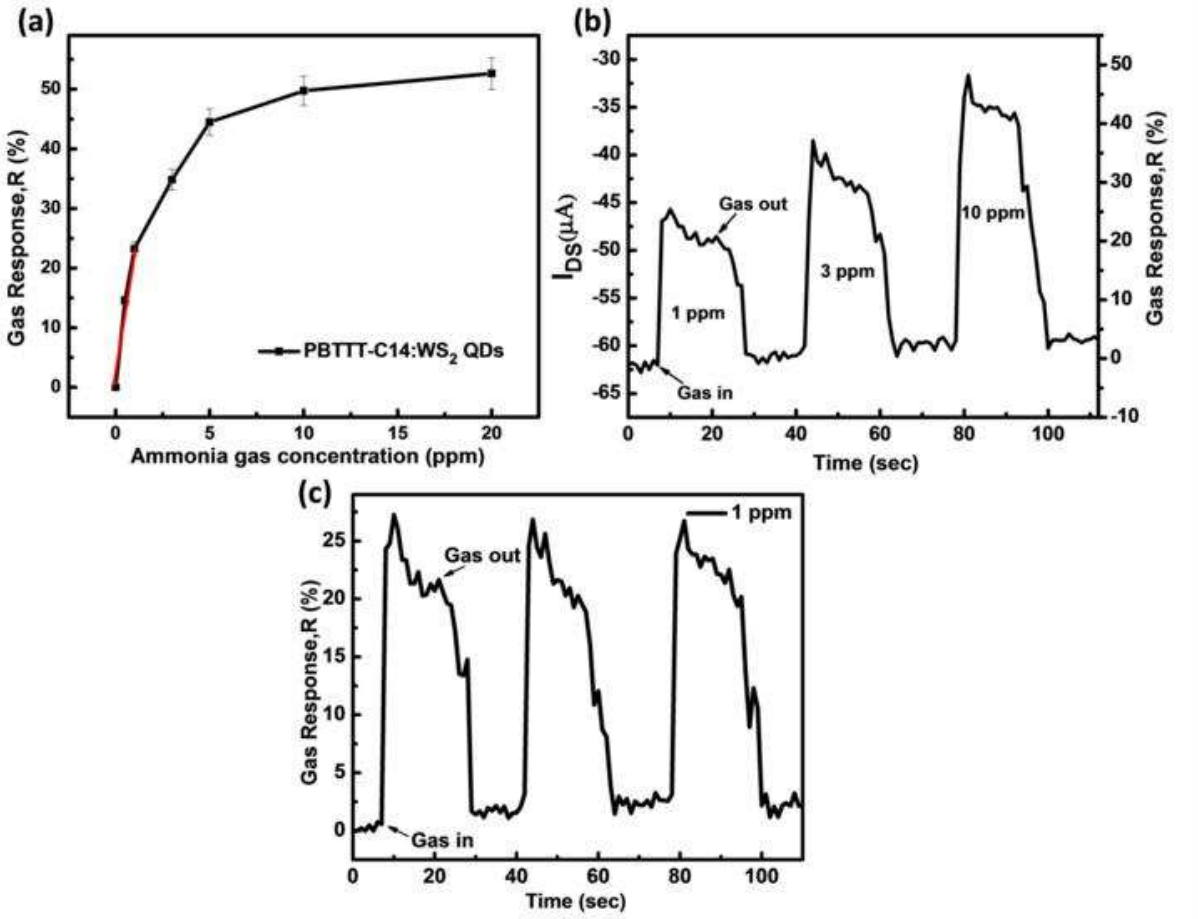

Fig. 4.5. (a) Estimation of detection limit (linear fitting of Gas response/calibration curve (red line)), (b) Transient gas response, and (c) repeatability of the TFT-based gas sensor at various concentration analyte gas at V_{DS} = -30 V and V_{GS} = -30 V.

In addition, the PBTTT-C14/WS_2-QDs based sensor has been tested for its reversibility characteristics, which is performed by repeated NH_3 flow with a fixed concentration in a certain time interval. Fig. 4.5(c) represents the transient response (V_{DS} = -30 V and V_{GS} = -30 V) for 1 ppm concentration of ammonia, which shows almost similar gas response in each cycle. These characteristics illustrate the good repeatability of the device, indicating its high reliability for practical application. A comparative performance of the PBTTT-C14/WS_2-QDs based OTFT sensor w.r.t the earlier reports are given in the Table-4.2.

Comparative performance of the PBTTT-C14/WS_2-QDs heterojunction based TFT sensor w.r.t the earlier reports are given in the Table-4.2.

Sensing material	Device Type	Gas concentration	Response	Response/ Recovery time	Remark
PQT-12	MSM	100 PPM	8%	8s/103s	Poor sensitivity [24]
Tips - Pentacene	OTFT	10 PPM	25%	200s/400s	Poor response/ recovery [159]
P3HT/RGO	OTFT	100 PPM	0.8%	5min/5min	Very low sensitivity [160]
PBTTT/MoS_2 -QDs	OTFT	50 PPM	Acc. Mode res.- 84.66% , dep. mode (Off current factor)- 3X 10^3	2s/-	Not sensitive for lower concentrations [161]
PBTTT/WS_2 -QDs (This work)	OTFT	20 PPM	Acc. Mode res.- 52.62%, dep. mode (Off current factor)- ~ 10^3	2s/6s	Quick response and recovery

4.3.6. Selectivity and Humidity Analysis

The selectivity study of the gas sensor is a crucial issue that helps us to recognize that particular analyte if it is mixed in with a similar type of analyte. Alternatively, it can be defined as the sensor's ability to detect a particular gas in presence of the other oxidative, reductive, and other common interfering gases. Fig. 4.6(a) represents the selectivity data of this heterojunction nano-composite based ammonia sensor. This data implies that the TFT based sensor having a higher response (positive) at 20 ppm NH_3 concentration compared to the other interfering gases, such as carbon dioxide (CO_2), carbon monoxide (CO), methane (CH_4), and propane (C_3H_8), which have been investigated up to 50 ppm of concentrations. In the characteristics, CH_4 gas possess positive response but with a negligible value. However, the other gases as CO_2, CO, and C_3H_8 are showing negative response (negligible) toward the sensor. This comparative data is ascribed to the high electron-donating capacity of the NH_3 gas, as discussed in the later mechanism section. However, for the other, gases the response value of the sensor either positive or negative, which depends on the electron-donating or capturing capability of the analyte gas [156, 162, 163].

Besides, it is very important to examine the influence of relative humidity on this ammonia sensor. For this investigation, the sensor has been exposed with 3 ppm concentration of ammonia in different RH ranges, and the findings are displayed in Fig. 4.6(b). This data implies that the variations in RH have a very mild effect on the sensor's response (V_{DS} = -30 V and V_{GS} = -30 V) as the drain current changes only 5% during the variation of RH from 20 to 80% as illustrated in the inset of Fig. 4.6(b). These outcomes suggest that the PBTTT-C14/WS_2-QDs heterojunction based TFT ammonia sensor is an excellent choice for NH_3 detection within a broad humidity range at room temperature.

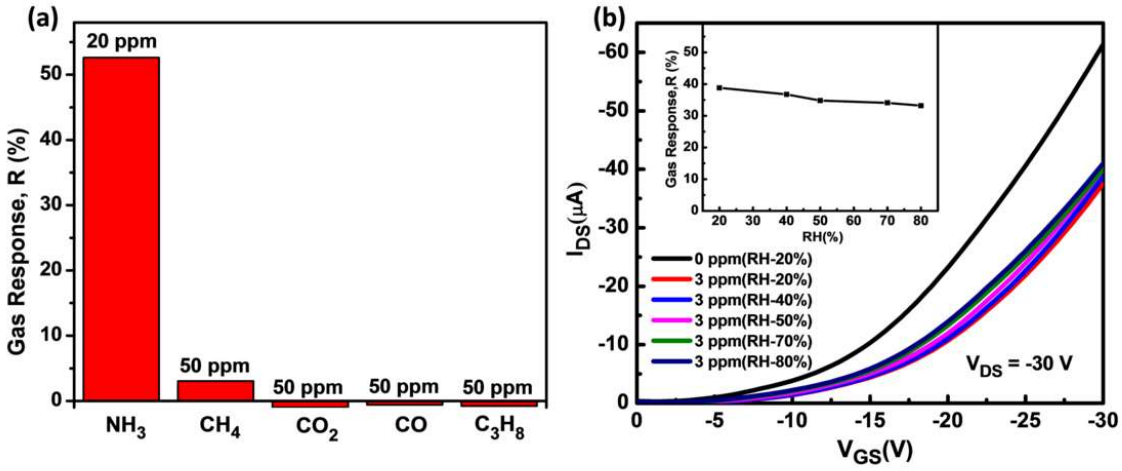

Fig. 4.6. (a) Selectivity analysis of sensor among various interfering gases, (b) Gas response of the TFT sensor with the variation of RH.

4.3.7. Ammonia sensing mechanism

The mechanism of ammonia detection by this PBTTT-C14/WS_2-QDs heterojunction based TFT sensor can be recognized from the variation of depletion layer and associated barrier height of polymer/QDs heterojunction. In this heterojunction WS_2-QDs and PBTTT-C14 works as n- and p-type semiconductors that forms a depletion layer around the junction where 'holes' transfer from the polymer to the QDs and 'electron' in a reverse way until their Fermi level achieved thermal equilibrium. As a consequence, a potential barrier will form at the heterojunction through this charge transfer (Fig. 4.7(b)). This uniformly distributed depleted part of this film exists throughout this nano-composite thin film (Fig. 4.7(a)). Electron-donating (reductive) NH_3 gas [135], decreases the hole concentration in the exposed polymer film, resulting in an extended depletion layer of the heterojunction, as shown in Fig. 4.7(c). Consequently, the PBTTT-C14 polymer's net mobile charge carrier concentration decreases, resulting in an enhancement of the total sheet resistance of the TFT channel. The potential barrier height of the mobile charges also

likewise increases (Fig. 4.7(d)). As a result, effective mobile carrier concentration of the polymer/QDs heterojunction thin film reduces.

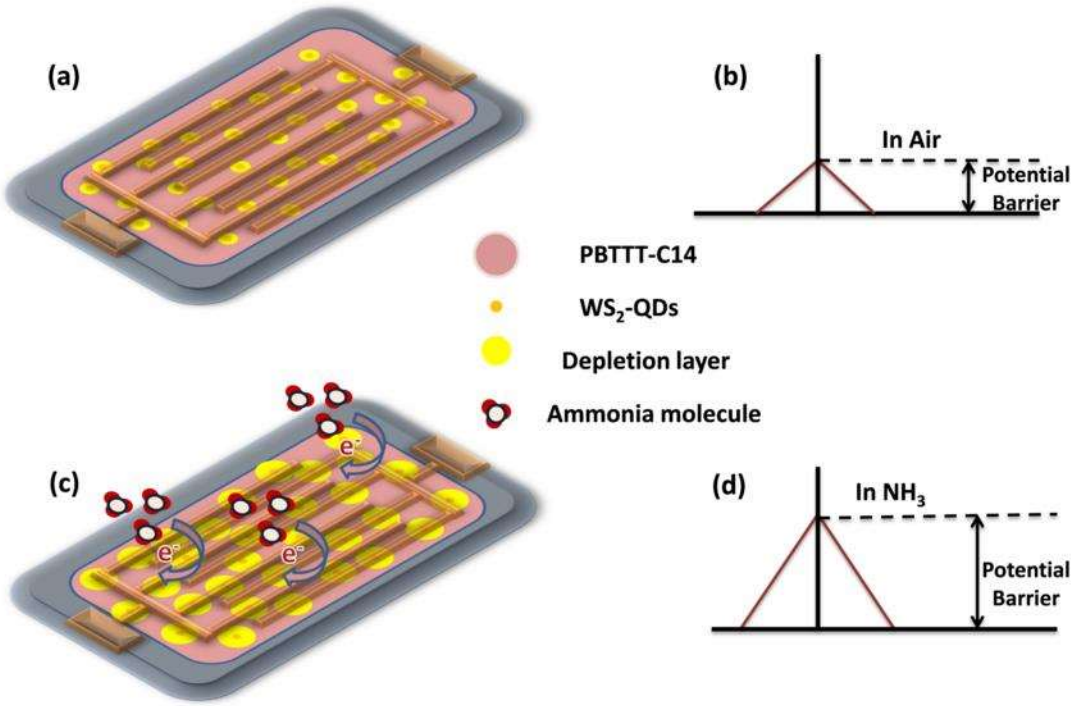

Fig. 4.7. Sensing mechanism of the TFT based sensor before and after the exposer of NH_3 gas.

As a consequence, TFT parameters, such as the ON/OFF ratio, carrier mobility (μ), and threshold voltage (V_{th}) changes continuously with gas concentration. There are two key factors that influence the OFF current of a TFT. The first is the gate-leakage current, and the second is the channel's DC conductance. If conductance of the polymer/QDs film decreases during the gas exposure and the gate leakage current of the TFT remains unchanged, then the off current of the TFT should decrease. Figure 4.8(a) demonstrates the OFF current variation of the TFT sensor, which diminishes gradually with increasing NH_3 concentration, supporting the enhancement of the polymer/QDs heterojunction depletion layer. Therefore, the 'OFF current factor' (ratio of OFF current before and after the exposer of NH_3) of the device, which is depicted in Fig. 4.8(b)

increases with gas concentration. Moreover, the variation in OFF current factor for device is ~10^3 orders greater than the device's on current variation. Besides, the semi-log presentation of this 'OFF current factor' has a good linearity with the analyte gas concentration. It can be noted that the variation of this 'OFF current factor' in the concentration range of 0-20 ppm is ~10^3, whereas in our earlier work, within this range it was only ~20 time, which indicates the level of improvement of this current work [156]. On the other hand, this sensor is capable to detect NH_3 gas within 20 ppm concentration and above of this range, variation of this 'OFF current factor' is very less.

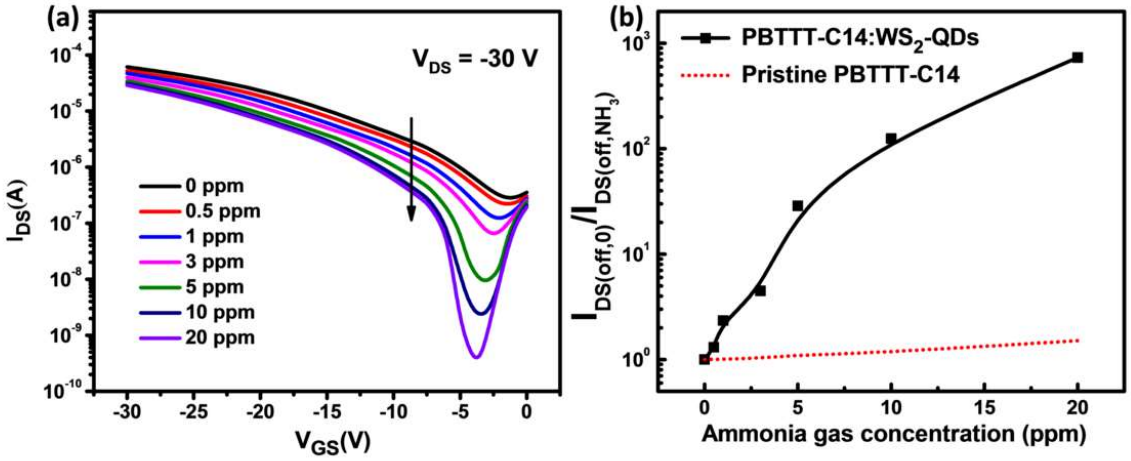

Fig. 4.8. (a) OFF current variation in nanocomposite based TFT sensor, and (b) variation of 'OFF current' factor with the NH_3 concentration in pristine PBTTT-C14 and PBTTT-C14/WS_2-QDs based TFT sensors.

In contrast, the earlier reported device is capable of measuring up to 50 ppm concentration by maintaining its good linearity [156]. Besides, off current factor data of reference pristine PBTTT-C14 based TFT has been presented in a dotted black line. From Fig 4.8(b), it can be observed that the improvement of off current factor w.r.t the pristine TFT is several orders

higher throughout the range. In addition to the OFF current variation of the device, the enhanced depletion layer enhances the depleted charge accumulation at the interface of dielectric and semiconductor, resulting in a shift in the V_{th} of the device by 6 V. As a consequence of this depleted charge accumulation of the polymer/QDs heterojunction, the effective carrier mobility of the TFT likewise decreases from 0.054 to 0.043 $cm^2 V^{-1}sec^{-1}$.

4.3.8. Broadband photo sensing properties

In addition to the NH_3 sensitivity, we also investigated the photo-sensing properties of fabricated polymer/QDs heterojunction based TFT under white light illumination in ambient conditions. A relative energy band diagram of this p-n heterojunction has been presented in Fig. 4.9(a) that represents a type-II heterojunction. Fig. 4.9(b) represents the UV-Vis absorption spectra of the pristine PBTTT-C14 and PBTTT-C14/WS_2-QDs nano-composite thin films, within the range of 300 to 1600 nm (QE-R quantum efficiency system (ENLITECH)). From these comparative absorption spectra, it can be noted that the absorption of the PBTTT-C14/WS_2-QDs film is mostly due to the PBTTT-C14 and is limited within 350 to 600 nm. The signature of the WS_2-QDs is quite invisible due to the lower concentration of the QDs in the polymer. However, these WS_2-QDs have a big role for the enhancement of photosensitivity that forms a depletion layer in the interfaces of the heterojunction as described earlier. Therefore, the performances of the polymer/QDs based phototransistors were investigated under white light illumination.

Fig. 4.10(a) shows the electrical characteristics of fabricated polymer/QDs based phototransistors under various white light intensities varied from dark to 650 W/m^2. This electrical data implies a large improvement in both (ON and OFF) the currents and is due to the photocurrent generation

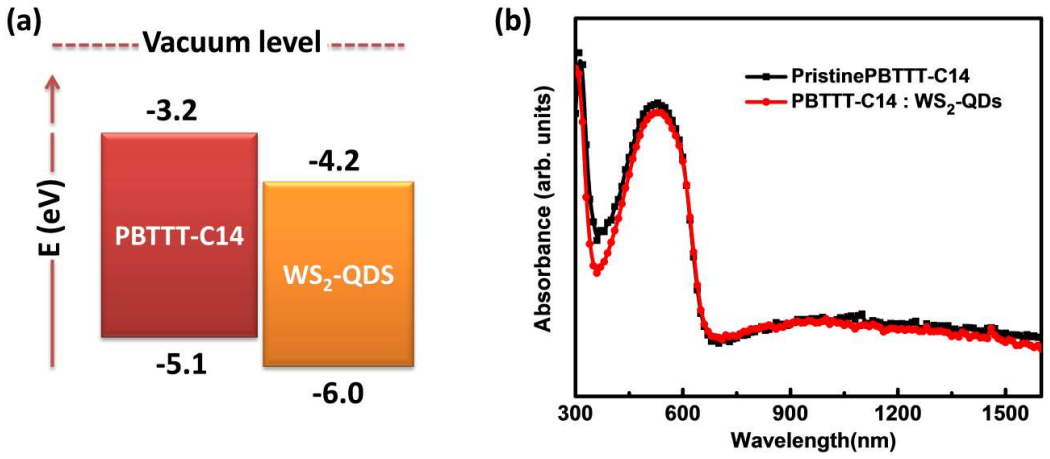

Fig. 4.9. (a) Energy level diagram of PBTTT-C14/WS_2-QDs, (b) UV-Vis spectra of PBTTT-C14 and PBTTT-C14/WS_2-QDs nano-composite.

in the hybrid channel of TFT. This data also indicates that there is ~ 70 times enhancement of OFF current under 650 W/m^2, whereas ON current of the device has been increased only 2.2 times (Fig. 4.10(c)). This data suggests that OFF current variation of this TFT is larger, which is due to the formation of depletion layers at the interfaces of nano-composite heterojunction. The photo-generated carrier in this depleted area then transfers to the PBTTT-C14 polymer which causes a large enhancement of channel conductivity, resulting in a larger variation of the OFF current of the device. Besides, a large positive shift of threshold voltage has been observed which originated due to the enhancement of carrier concentration of the channel. Fig. 4.10(b) displayed the threshold voltage shift of the phototransistor under various white light intensities. The threshold voltage Shift is as large as ~22 V corresponding to the light intensity of 650 W/m^2.

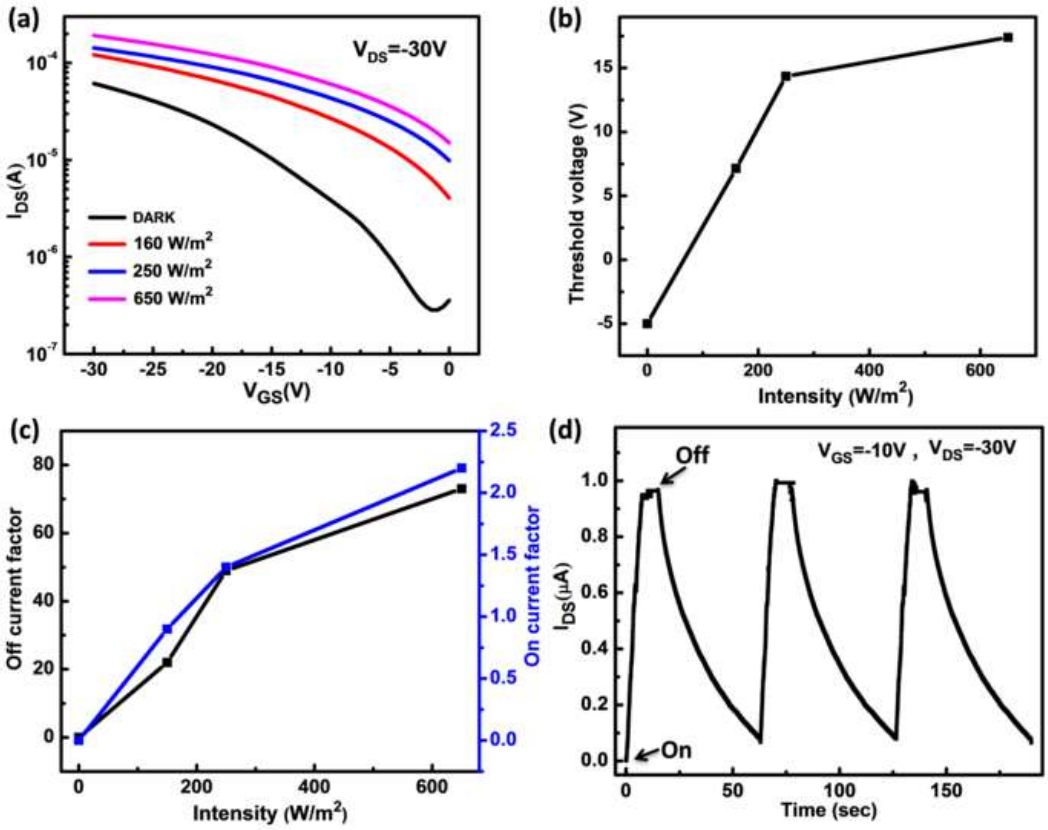

Fig. 4.10. (a) Output characteristics of heterojunction phototransistors (V_{DS} = -30 V) in dark and under various intensities of white light illumination, (b) Threshold voltage shift of the phototransistor under various white light intensities, (c) ON-state and OFF-state current factor and (d) Transient photo current response of the fabricated phototransistor at V_{DS} = -30 V and V_{GS} = -10 V.

The transient photo response of the heterojunction based phototransistor is represented in Fig. 4.10(d), which indicates the device has a faster response but a longer decay time. The primary reason of this longer decay time depends on the transit time of photo-generated carrier, which depends on two primary factors. One is the channel length of TFT and the other one is the carrier mobility of the semiconductor. This PBTTT-C14/WS_2-QDs has relatively poor carrier mobility.

Besides, the channel length is ~50 μm, which is quite high. Therefore, decay time is also very long. For this particular PBTTT-C14/WS_2-QDs semiconductor based TFT, the decay time can be faster if we reduce the channel length.

4.4. Conclusion

A highly sensitive PBTTT-C14/WS_2-QDs nano-heterojunction TFT based NH_3 sensor and broadband photo-detector has been fabricated by a simple, economical and high yield 'FTM procedure'. Hydrothermally synthesized WS_2-QDs and PBTTT-C14 blend based thin film has been used as the active NH_3 sensing layer of the TFT device. A considerable change in the ON current of the device has been noticed due to the small variation in gas concentration, which leads to the significant change in device parameters and consent to get a response of 50% at 10 ppm NH_3 concentration. Additionally, sensor based on PBTTT-C14/WS_2-QDs exhibited rapid response and recovery following each gas pulse with exceptional sensitivity and repeatability. Again the variation of this 'OFF current factor' in the concentration range of 0-20 ppm is ~10^3, whereas in our earlier PBTTT-C14/MoS_2-QDs work, within this range, it was only ~20 times with poor NH_3 recovery mechanism, which indicates the level of improvement of this current work. This TFT also possesses superior selectivity and can detect the low concentrations of NH_3 up to the detection limit of 0.44 ppm. Besides, around 70 times OFF current variation of this TFT has been observed under 650 W/m^2 white light illumination, indicating its very high photosensitivity under white light. In short, this PBTTT-C14/WS_2-QDs nano-heterojunction based TFT acquires very high sensitivity with fast response/recovery times with a wide range of detection capabilities, and is meeting most of the fundamental requirements for its practical implementation as an NH_3 sensor and broadband photo-detector.